Dehydroglutathione to induce non-reducible glutathionylation for functional analysis

Daniel Oppong,[1] Rayavarapu Padmavathi,[1] Dhanushika S. K. Kukulage,[1] Madhu C. Shivamadhu,[1] Elizabeth A. Newberry,[1] Anneliese M. Faustino,[2] Hsin-Yao Tang,[2] and Young-Hoon Ahn[1]*

[1]Department of Chemistry, Drexel University, Philadelphia, PA 19104, USA

[2]The Wistar Institute, Philadelphia, PA 19104, USA

Corresponding author: Young-Hoon Ahn, ya426@drexel.edu; (215) 895-2666

Running title: Dehydro-glutathione to induce a glutathionylation mimic for functional studies.

Keywords: glutathionylation, dehydroglutathione, redox signaling, FABP5, cell migration.

Abstract

Protein cysteine is susceptible to diverse oxidations, including disulfide, S-sulfenylation, S-nitrosylation, and S-glutathionylation, that regulate many biological processes in physiology and diseases. Despite evidence supporting distinct biological outcomes of individual cysteine oxoforms, the approach for examining functional effects resulting from a specific cysteine oxoform, such as S-glutathionylation, remains limited. In this report, we devised a dehydroglutathione (dhG)-mediated strategy, named G-PROV, that introduces a non-reducible glutathionylation mimic to protein with the subsequent delivery of the modified protein to cells to examine “phenotype” attributed to “glutathionylation”. We applied our strategy to fatty acid binding protein 5 (FABP5), demonstrating that dhG induces selective modification at C127 of FABP5, resembling S-glutathionylation. dhG-modified glutathionylation in FABP5 increases its binding affinity to linoleic acid, enhances its translocation to the nucleus for activating PPARβ/δ, and promotes MCF7 cell migration in response to linoleic acid. Our data report a facile chemical tool to introduce a glutathionylation mimic to protein for functional analysis of protein glutathionylation.

Introduction

Cysteine in proteins is unique for its high nucleophilicity and oxidation-susceptibility.[1, 2] These features render protein cysteines to exert distinct biological functions, such as redox sensing.[1, 3] Cysteine oxidations occur in response to diverse biological, medical, and environmental factors, including growth factors and cytokines,[4-6] reactive oxygen species (ROS),[7] nutrients,[8-10] chemotherapy,[11, 12] radiation,[13] and metals,[14, 15] suggesting their prevalence and significance in biology and medicine. The complexity of cysteine oxidations is that cysteine forms diverse oxoforms, including S-sulfenylation, disulfide formation, S-glutathionylation, and S-nitrosylation, which retain unique structures and chemical reactivity.[3] Although different cysteine oxoforms could cause similar functional outcomes (e.g., inhibiting enzyme activity), evidence supports that individual cysteine oxidations occur on distinct sets of proteins and regulate different biological pathways and processes,[16] warranting investigation of individual cysteine oxidations.

Protein S-glutathionylation is one of the main cysteine oxidations and represents protein cysteine disulfide bond formation with intracellular glutathione.[17] The significance of protein S-glutathionylation has been demonstrated with its regulatory or contributing roles in physiology and pathology,[17, 18] including proliferation, migration,[4, 19] inflammation,[20] fibrosis,[21] the cardiovascular system,[22, 23] neurodegeneration,[24] and cancers,[25] among others. It is notable that the development of biochemical tools and strategies, especially in conjugation with proteomics and mass spectrometry, enabled the identification of a large number of proteins and cysteines (n>2,000) susceptible to S-glutathionylation.[17] The cysteine sites identified via proteomics serve as important

candidates for uncovering the biological functions upon their glutathionylation.[4] However, the general strategy for functional analyses relies on comparing biological phenotypes between two cohorts of cells expressing wild-type (WT) or Cys mutants (e.g., Cys to Ser or Ala) of a protein of interest (POI), i.e., mutating an oxidizable Cys residue.[4, 26, 27] Although effective, the approach concludes that biological functions are attributed to the POI's "oxidation" per se while there is a lack of direct evidence linking the POI's "glutathionylation" to biological phenotypes.

To address the limitation, we devised a strategy in this report, named "dhG-induced protein glutathionylation and delivery" (G-PROV) (Figure 1). The strategy involves two steps: (1) introducing a non-reducible glutathionylation mimic to POI using dehydroglutathione (dhG) (step 1) and (2) delivery of the modified POI to cells (step 2) where the functional effects of POI with a glutathionylation mimic can be investigated. We applied our strategy to fatty acid binding protein 5 (FABP5). FABP5 is one FABP isoform that plays an important role in lipid transport and metabolism.[28] FABP5 is implicated in metabolic syndrome, neurologic diseases, inflammation, and cancers.[28, 29] Previous studies showed that FABP5 is a redox-active protein, forming intracellular disulfide and S-glutathionylation.[30-32] Functional analysis demonstrated that FABP5 S-glutathionylation suppresses lipopolysaccharide-induced inflammation in macrophages.[31] In this study, we showed that the G-PROV strategy induces a glutathione modification in FABP5, resembling S-glutathionylation. We demonstrated that dhG-derived glutathione modification in FABP5 increases its binding affinity with linoleic acid (LA), activates peroxisome proliferator-activated receptor β/δ (PPARβ/δ), and increases migration of MCF7 cells upon incubation of LA. Our report provides a new facile strategy for the

functional study of protein glutathionylation while providing evidence linking “FABP5 glutathionylation” to “cancer cell migration.”

Result

dhG generates a glutathione modification on Cys resembling glutathionylation.

dhG contains dehydroalanine (dhA) instead of L-Cys in glutathione (γGlu-Cys-Gly).[33] The Michael acceptor in dhG can react with protein cysteine to form a protein-glutathione conjugate with a thioether linkage (P-SG) in place of disulfide (PS-SG) in glutathionylation. While the P-SG differs from PS-SG such that it lacks one sulfur atom and likely loses stereochemistry at the Cys in glutathione, we envisioned it is a close mimic to glutathionylation and non-reducible, and it may induce similar functional effects to glutathionylation.

dhG was synthesized in two steps from glutathione (Figure S1A).[33] dhG was then tested for its reaction with cysteine. The incubation of dhG with N-acetylcysteine (NAC) in PBS resulted in the Michael reaction product containing the thioether bond (Figure 2A) confirmed by NMR (Figure S1B). Next, dhG was examined for its reaction with a Cys-containing 16-mer peptide (PEP: AVMNNVTCTRIYEKVE. The sequence is derived from the redox active C127 in FABP5 with neighboring amino acids) (Figure 2B). PEP reaction with dhG also generated the Michael reaction conjugation product confirmed by mass spectrometry (Figure S1C), suggesting the selective reaction of dhG with Cys. The reactions of Michael acceptors, such as an acryl group, with thiols proceed at high rates (the second-order rate constant 0.25-65.0 $M^{-1}s^{-1}$).[34] Therefore, we monitored the reaction kinetics of dhG with fluorescein-conjugated PEP (FAM-PEP) (Figure 2B, top). To

measure the reaction rate, FAM-PEP conjugation with dhG (over 10-fold excess, pH 8.0) was monitored over time in the urea-based gel electrophoresis (Figure 2B, bottom).[35] FAM-PEP showed time- and dose-dependent dhG conjugation (Figure S1D) with the second-order rate constant of 53.6 $M^{-1}min^{-1}$ (Figure 2C). The kinetics indicates a half-life ($t_{1/2}$) of FAM-PEP is 12.9 min (with 1 mM dhG), suggesting 90% conversion in <1 h. These experiments confirm that dhG selectively reacts with Cys, leading to a thioether-based glutathione modification on Cys.

dhG induces a glutathione modification at Cys127 of FABP5

To evaluate dhG with protein, we selected FABP5, known for its cysteine oxidation. FABP5 has six cysteines (Figure 3A), among which C120 and C127 are in proximity (4.4 Å) and susceptible to disulfide bond formation,[30, 32] and C127 is reported to form S-sulfenylation[36] and S-glutathionylation,[17, 31] suggesting C127 as a redox-active cysteine.

We expressed and purified FABP5 from *E. coli*, and bound lipids were removed by delipidation (Figure S2). The dhG incubation with FABP5 caused dhG concentration-dependent modification detectable by glutathione antibody (Figure 3B). dhG modification in FABP5 was not reduced upon DTT treatment, whereas the same DTT treatment reduced the level of S-glutathionylation in FABP5 induced by GSSG (Figure S3A), confirming a non-reducible nature of dhG modification in FABP5.

To analyze modified cysteines, FABP5 WT and individual cysteine mutants were compared. dhG induced glutathione modification in C120S and C87S with comparable levels to WT, whereas dhG modification in C127S was significantly reduced compared to WT (Figure 3C), suggesting that C127 is a major cysteine for dhG modification. Next, dhG

modification was compared with S-glutathionylation. FABP5 constructs incubated with oxidized glutathione (GSSG) showed a similar pattern as dhG, such that FABP5 C127S has a reduced signal of S-glutathionylation compared to WT, C120S, and C87S (Figure 3D).

To confirm dhG-modified cysteine sites, FABP5 constructs without and with dhG incubation were analyzed by MALDI-TOF. The analysis showed that dhG induced +273 Da addition to FABP5 WT (18,641 vs. 18368 Da with and without dhG. Expected mass change: +273.10 Da) (Figure 3E, left middle), whereas no significant change was observed with C127S (18,356 vs. 18,357 Da with and without dhG) (Figure 3E, right middle). In comparison, the incubation of GSSG caused +305 Da addition to FABP5 WT (18,673 vs. 18,368 Da with and without GSSG. Expected mass change: +305.2 Da) (Figure 3E, left, bottom) without observing a significant mass change with FABP5 C127S (18,355 vs. 18,357 Da with and without GSSG) (Figure 3E, right, bottom). Subsequently, FABP5 WT modified by dhG was digested by cyanogen bromide (CNBr). The MALDI-TOF analysis of the fragmented mixture identified the mass matching to a peptide modified with dhG at C127 via Michael addition (NNVTC*TRIYEKVE, m/z 1842 Da) (Figure S3B). The subsequent LC-MS/MS analysis confirmed dhG modification at C127 (Figure 3F). These experiments support that FABP5 C127 is the most susceptible to dhG modification via the Michael reaction, generating a thioether form of non-reducible glutathione modification in FABP5. dhG modification occurs in the same cysteines as S-glutathionylation in FABP5.

FABP5 dhG modification increases its binding affinity to fatty acid

FABP5 has a twisted β-barrel structure, comprised of two β-sheets arranged by ten β-strands, and two helices (α1 and α2) acting as a lid on top of the β-barrel (Figure 3A).[32] A fatty acid binds to the inner space of the β-barrel with U- or L-shape conformation (Figure 3A, right),[37] by which the helical lid moves in or out from the β-barrel core, increasing or decreasing α2 helix interaction with a βC-βD loop (i.e., M35 and L60).[37] C127 is relatively hidden in the β-barrel core, albeit close to the helix lid (Figure 3A). Interestingly, FABP5 C127 S-glutathionylation was shown to increase its binding affinity to linoleic acid (LA) in a biochemical pull-down experiment.[31] To demonstrate the functional similarity of FABP5 dhG modification to S-glutathionylation, we examined the binding affinity of FABP5 with LA after dhG modification or S-glutathionylation.

The isothermal titration calorimetry (ITC) experiment demonstrated that FABP5 WT binds to LA with a K_D value of 2.2 ± 1.1 μM (Figure 4A, left, and 4C). In contrast, after dhG modification, FABP5 WT displayed ca. 3-fold higher binding affinity (K_D = 0.74 ± 0.05 μM) (Figure 4A, right, and 4C), consistent with the observation that FABP5 S-glutathionylation increases its binding with LA.[31] However, after GSSG incubation, FABP5 WT displayed binding affinity (K_D = 2.4 ± 6.1 μM) similar to non-glutathionylated FABP5 WT (Figure 4C and S4). The discrepancy was hypothesized that FABP5 WT S-glutathionylation at C127 may have caused C120 to displace the glutathione on C127, forming an intramolecular disulfide during purification steps. To remove the complication resulting from C120/C127 disulfide, we analyzed FABP5 C120S. FABP5 C120S retained similar binding affinity (K_D = 2.3 ± 2.1 μM) (Figure 4B, left, and 4C) comparable to FABP5 WT, suggesting C120S mutation does not cause a significant change in its binding to LA. FABP5 C120S increased its binding affinity to LA after dhG modification (K_D = 0.71 ± 0.03

μM) (Figure 4B, right, and 4C) or GSSG incubation (K_D = 0.66 ± 0.05 μM) (Figure 4C and S4). The increased binding energy (ΔG = -8.4 vs. -7.7) of FABP5 WT with LA upon dhG modification is driven by more favorable enthalpy (ΔH = -4.0 vs. -1.0) and less unfavorable entropy (ΔS = -4.3 vs. -6.6) (Figure 4D, bars 1 vs. 2). FABP5 C120S showed the essentially same thermodynamic changes as WT upon dhG modification (Figure 4D, bars 4 vs. 5). In addition, GSSG-induced S-glutathionylation caused the same thermodynamic changes as dhG modification in FABP5 C120S (Figure 4D, bars 6 vs. 5). These experiments support that FABP5 C127 glutathione modification increases the binding affinity to LA, and dhG-induced FABP5 glutathione modification exhibits comparable functional effect to FABP5 S-glutathionylation.

FABP5 glutathione modification increases its nuclear level and PPARβ/δ activation

The second step of our G-PROV strategy is to deliver the dhG-modified POI to cells (Figure 1). To do so, we used fusogenic liposome, which has been demonstrated to deliver cargo protein to the cytoplasm via fusion with the plasma membrane, as opposed to lysosome or endosome via endocytosis.[38] First, we analyzed the delivery of FABP5 to MCF7 cells, which have a low level of endogenous FABP5.[39] The fusogenic liposome containing FLAG-FABP5 was incubated with MCF7 cells (1 h). The immunostaining of FLAG-FABP5 was found largely distributed in the cytoplasm without localizing to the nucleus, while the FLAG-signal was minimally overlapped with the endosome marker Rab9A (Figure S5A),[40] supporting that FABP5 was delivered mostly to the cytoplasm but with its low level at the endosome/lysosome.

The cellular delivery of FLAG-FABP5 constructs via fusogenic liposomes was also analyzed in lysates. The western blot analysis by FLAG-antibody found that the same amounts of four constructs (FABP5 WT and C127S without and with dhG) were delivered to cells (Figure 5A, FLAG). In contrast, glutathione modification is mainly found in cells with FABP5 WT incubated with dhG (FABP5 WT-SG), along with its low level in FABP5 C127S incubated with dhG (FABP5 C127S-SG) (Figure 5A, lanes 2 vs. 1, 3, 4). Notably, one distinct protein band, corresponding to FABP5 molecular weight, shows a strong signal for glutathione modification (Figure 5A, lane 2), suggesting that mainly a single protein, FABP5, retains a significant level of glutathione modification in the whole proteome.

FABP5 upon binding to LA generates its non-canonical nuclear localization signal.[37] FABP5 was previously shown to increase its translocation to the nucleus in response to H_2O_2,[31] implying that FABP5 S-glutathionylation increases its binding to LA and enhances its nuclear localization. The translocated FABP5 interacts with PPARβ/δ for transcriptional activation.[41] Therefore, the nuclear levels of four FABP5 constructs in response to LA were examined by detecting FABP5 in the nuclear lysates after cell fractionation. FABP5 WT-SG did not show its increased nuclear level, compared to FABP5 WT, without adding LA (Figure 5B, lane 3 vs. 2). However, FABP5 WT-SG was more significantly found in the nuclear extract than FABP5 WT upon adding LA (Figure 5B, lane 6 vs. 5), suggesting the enhanced translocation of FABP5 upon dhG modification. Lastly, The PPARβ/δ transcriptional activation was examined. The PPARβ/δ activation assay showed that FABP5 WT and FABP5 WT-SG activate PPARβ/δ at comparable levels without adding LA (Figure 5C, bars 3 vs. 2). However, in the presence

of LA, FABP5 WT-SG induced higher PPARβ/δ activation than FABP5 WT (Figure 5C, bars 6 vs. 5). These experiments support that dhG-modified FABP5 glutathionylation increases nuclear translocation and PPARβ/δ activation.

FABP5 glutathione modification increases cell migration

The PPARβ/δ activation induces higher migration, invasion, and metastasis of cancer cells.[29, 42, 43] Therefore, we analyzed the migration of MCF7 cells containing FABP5 constructs upon adding LA. The in vitro scratch migration assay showed that MCF7 cells containing FABP5 WT or FABP5 WT-SG showed comparable levels of cell migration in the absence of LA (Figure 5D, bars 3 vs. 2). However, upon incubating LA, FABP5 WT-SG induced higher cell migration than FABP5 WT (Figure 5D, bars 6 vs. 5). To see the importance of C127 for glutathione modification, we analyzed FABP5 C127S without and with glutathione modification by dhG. Unlike FABP5 WT, FABP5 C127S and FABP5 C127S-SG induced similar levels of MCF7 cell migration in the presence and absence of LA (Figure 5E, lanes 2 vs 3, and 5 vs. 6 and S5B), supporting that FABP5 C127 glutathione modification is responsible for the observed increase in cell migration.

Discussion

S-glutathionylation is emerging as an important redox-regulatory event in pathophysiologic processes.[17] Although a large number of S-glutathionylated proteins were identified via proteomics, the functional annotation of the identified S-glutathionylated cysteines remains still limited.[17] In this report, we developed a strategy named G-PROV that installs glutathione modification on a protein of interest (POI) with

its subsequent delivery to cells, where the functional effects of “glutathione” modification of POI can be probed. It is worth stating that the proteome in cells largely stays in a reduced state at a basal (non-stressed) condition. Therefore, the cellular delivery of POI modified by dhG via the fusogenic liposome rendered cells, where only POI retains a significant glutathione modification in the proteome, and the effect of glutathionylation on a single protein can be investigated. Therefore, the G-PROV approach helps determine “phenotype” changes resulting from POI “glutathione” modification.

Previously, the “Tag-and-Modify” approach for converting cysteines in a recombinant protein to dehydroalanine (dhA) (e.g., using diethyl *meso*-2,5-dibromo adipate) was developed.[44, 45] Subsequently, dhA in a protein could be further derivatized to diverse post-translational modifications (PTMs), including glutathionylation.[44] Therefore, the “Tag-and-Modify”-mediated non-reducible glutathione modification in proteins is feasible,[44] but the approach typically accompanies mutations of other cysteines than cysteines of interest. In addition, the two-step process may involve additional purification steps. As an alternative, the G-PROV strategy demonstrates a simple one-step for glutathione modification in protein combined with a strategy for its cellular delivery for functional analysis. However, it is important to note that the Michael reaction between dhG and cysteine in protein generates glutathione modification with a loss of stereochemistry in Cys of glutathione and one atom shorter than S-glutathionylation. Although we demonstrate that dhG-modification in FABP5 induces similar functional changes to S-glutathionylation, it is possible that dhG-mediated glutathione modification could cause biochemical changes deviating from S-glutathionylation.

FABP5 has six cysteines (C43, C47, C67, C87, C120, and C127). The six cysteines are partially conserved in the FABP family, and FABP5 is the only member in the FABP family with six cysteines. C120-C127 disulfide was found previously,[32] and C67-C87 are in proximity without forming the disulfide.[32] In addition to intramolecular disulfide, C127 was found for S-sulfenylation[46] and S-glutathionylation,[31] suggesting its tendency to form multiple oxoforms with high nucleophilicity and oxidation susceptibility. In this report, we introduced a glutathione modification mainly at C127 in FABP5. The ITC experiment showed that dhG-modified or GSSG-mediated glutathionylation in FABP5 at C127 increases ca. 3-4-fold binding affinity. Interestingly, the increase of the binding affinity (more negative ΔG) is attributed to the enthalpy increase (more negative ΔH) in addition to the more favorable entropy (more positive ΔS), suggesting that glutathione could form additional interactions with LA directly or via a network of water molecules in a pocket. Thus, the data imply that the increased binding affinity of FABP5 may result from glutathione modification per se rather than other oxoforms. However, it remains to be seen whether other oxoforms of C127 can increase FABP5 binding affinity to LA. Lastly, we demonstrate that FABP5 glutathione modification increases MCF7 cell migration via activating PPARβ/δ. Because FABP5 is involved in activating many transcription factors and oncogenes (e.g., NF-kB),[29] it would be necessary to see whether FABP5 glutathionylation regulates other signaling pathways.

Experimental Methods

Protein purification. pET2a-FABP5 wild-type plasmid was a gift from Dr. Martin Kaczocha at Stony Brook University. FABP5 mutants (C127S, C120S, and C87S) were

generated using site-directed mutagenesis (C87S forward primer: 5'-GCAGAAAAACTCAGACTGTCAGCAACTTTACAGATGGTG-3' and reverse primer: 5'-CACCATCTGTAAAGTTGCTGACAGTCTGAGTTTTTCTGC-3'; C120S forward primer: 5'-GAAATTAGTGGTGGAGAGCGTCATGAACAATGTCACC-3' and reverse primer: 5'-GGTGACATTGTTCATGACGCTCTCCACCACTAATTTC-3'; C127S forward primer: 5'-GTCATGAACAATGTCACCAGCACTCGGATCTATGAAAAAG-3' and reverse primer: 5'-CTTTTTCATAGATCCGAGTGCTGGTGACATTGTTCATGAC-3'). FLAG tag was inserted into FABP5 constructs to generate pET2a-FLAG-FABP5 plasmids using inverse-PCR (forward primer: 5'-GATGACGACAAGCATATGGCCACAGTTCAGCAGCTG-3' and reverse primer: 5'-GTCTTTGTAGTCCCCGCTGCCGCGCGGCAC-3'). FABP5 plasmids were transformed into BL21 (DE3) competent cells. A single colony was inoculated into 5 mL Luria Broth (LB) medium containing 50 μg/mL kanamycin and grown at 37 ºC for 16 h. 2.5 mL overnight culture was inoculated into 1 L LB medium containing 50 μg/ml kanamycin and grown at 37 ºC until OD_{600} reached 0.5. Protein expression was induced with 0.5 mM isopropyl β-D-1-thiogalactopyranoside (IPTG) and incubated at 18 ºC for 18 h. Cells were pelleted by centrifugation at 5,000 rpm and washed with cold Tris-HCl buffer. Cells were lysed using a French press with a lysis buffer (25 mM Tris, pH 7.4, 300 mM NaCl, 1 mM DTT, and Pierce protease inhibitor, pH 7.4). Clarified lysate was incubated with Ni-NTA agarose beads at 4 ºC for 2 h. Proteins were eluted using elution buffer (25 mM Tris, 75 mM NaCl, 300 mM imidazole, 1 mM DTT, pH 7.4). Pure fractions were combined and dialyzed in dialysis buffer (25 mM Tris, pH 7.4, 75 mM sodium chloride, 1 mM DTT, and 5% glycerol).

Protein delipidation. 100 mg of lipophilic Sephadex LH-20-100 (hydroxypropyl dextran with C13-C18 alkyne ethers, dry beads)[47] (Sigma, H6383) was activated by immersing in 500 µL of buffer (10 mM potassium phosphate, 150 mM potassium chloride, 0.2 g/L sodium azide, pH 7.4) in a 1.5 mL microcentrifuge tube, followed by shaking at 37 °C for 2.5 h. 500 µL of FABP5 (2 mg/mL) was mixed with the bead suspension. The protein bead mixture was shaken at 37 °C for 2 h. The beads were separated from the protein using a 0.22-µm Millipore Amicon filter. Two cycles of the treatment were carried out. Delipidated FABP5 was dialyzed in PBS (10 mM Na_2HPO_4, 1.8 mM KH_2PO_4, 2.7 mM KCl, 137 mM sodium chloride, 1 mM DTT, and 5% glycerol, pH 7.4). Lipid removal was confirmed by staining delipidated protein with iodine solution (0.5 mg I_2 in 1 mL chloroform) on a TLC plate.

FABP5 dhG modification or S-glutathionylation. To FABP5 protein (0.5 mg) in PBS (pH 8.0) (0.5 mL) containing 1 mM DTT was added 10 mM dhG or 5 mM GSSG. The reaction was incubated at room temperature for 12 h unless stated otherwise. Unreacted dhG and GSSG were removed through dialysis. dhG modification or S-glutathionylation was analyzed using Coomassie stain or western blot.

Mass spectrometry. For MALDI-TOF analysis, 50 µg of FABP5-SG or FABP5-SSG was dialyzed into Milli-Q water containing 0.1% TFA. 1 µL sample was mixed with 1 µL of 2-cyano-3-(4-hydroxyphenyl)-2-propenoic acid) (α-CHCA) matrix solution (10 mg α-CHCA in 1 mL methanol with 0.1% TFA). 1 µL sample was spotted on a MALDI plate and analyzed by MALDI-TOF (Bruker). For MS/MS analysis, 50 µg of FABP5-SG was treated

with CNBr (10 µL of a solution prepared by 10 mg CNBr in 0.5 mL of 0.5 N HCl). The sample was incubated for 12 h at room temperature. The sample was purified on a C18 ziptip, lyophilized, and resuspended at a concentration of 1 µg/µL in 0.1% trifluoroacetic acid with sonication. LC-MS/MS analysis was carried out with an Ultimate 3000 RSLCnano system (Thermo Scientific) coupled to an Orbitrap Eclipse mass spectrometer (Thermo Scientific). For the chromatographic separation, the column compartment temperature was set to 45 °C, and the flow rate was set to 0.200 µL/min. Buffer A consisted of 0.1% formic acid in Milli-Q water, and Buffer B consisted of 0.1% formic acid in acetonitrile.1 µg of the sample was loaded onto a trap column (nanoEase M/Z Symmetry C18, 100 Å, 120 µm x 20 mm, Waters) and washed for 10 min with Buffer A. The trap column was placed in line with the resolving column (nanoEase M/Z Peptide BEH C18, 130 Å, 75 µm x 250 mm, Waters) and separated using a linear gradient increasing from 5% to 30% B over 75 min, then from 30% to 80% B over 5 min, held at 80% B for 10 min at an increased flow rate of 0.300 µL/min, and equilibrated at 5% B for 10 min.

MS data were acquired in data-dependent acquisition mode using a cycle time of 3 s. For each cycle, the MS1 scan was performed in the Orbitrap at 120k resolution, and precursor ions with a charge state between 2+ and 8+ and a mass of 350 – 1800 m/z were isolated (1.4 m/z window) for fragmentation by higher-energy collisional dissociation (30%). MS2 scans were performed in the ion trap with a scan range of 200 – 1400 m/z, a maximum injection time of 35 ms, and the scan rate was set to Turbo mode. Dynamic exclusion was enabled at 20 s.

RAW files were searched with MaxQuant 2.6.5.0 against the UniProt human complete database downloaded 2024.10.05 (83,413 entries) plus a contaminant database. N-terminal acetylation and methionine oxidation were variable modifications. dhG addition to cysteine ($C_{10}H_{15}N_3O_6$, 273.09608) was used for the modification. All other parameters were left at default values. Peptide spectra matches were accepted at a 1% false discovery rate as determined by a reverse database search. Peptide modification was analyzed using Skyline software (version 24.1.0.199). dhG modification ($C_{10}H_{15}N_3O_6$, 273.09608) was input into the structural modification tab. All other parameters were left to default values. Peptide libraries were built by importing all msms.txt files into Skyline using a default spectral library cut-off score of 0.95. Raw files were imported to Skyline for peak picking. Peptides that showed dhG mass modification were identified.

Isothermal titration calorimetry. FABP5 was dialyzed into 25 mM Tris-HCl and 75 mM NaCl pH 7.4. The affinity of linoleic acid for FABP5 was measured in MicroCal ITC (Malvern). The syringe was filled with linoleic acid (1 mM in Tris-HCl buffer). The sample cell was filled with FABP5 (0.1 mM in Tris-HCl buffer). The reference cell was filled with Tris-HCl buffer. The sample cell and the syringe were first equilibrated to 25 °C, followed by an initial delay of 60 seconds before the first injection of 0.4 µL of linoleic acid into the sample cell for 4 seconds. For the remaining injections, a 2 µL volume of linoleic acid solution was injected into the sample cell for 4 seconds. The syringe was stirred continuously in the sample cell at 750 rpm. A total of 19 injections were performed with a spacing of 150 seconds. The binding data were analyzed using the MicroCal ITC software. A one-site binding model was fitted to the data to calculate the binding

parameters. The equilibrium dissociation constant (K_D), Gibbs energy (ΔG), enthalpy (ΔH), and entropy (TΔS) were determined from the curve.

Cell culture. MCF-7 cells were purchased from ATCC and maintained in EMEM medium supplemented with 10 % fetal bovine serum (FBS, Hyclone, Cytiva), penicillin (100 units/mL), and streptomycin (100 µg/mL) (Pen-Strep). Cells were maintained at 37 °C in 5 % CO_2 in a humid atmosphere.

Fusogenic liposome preparation. Stock solutions of 1,2-dioleoyl-sn-glycero-3-phosphoethanolamine (DOPE), *N, N, N*-trimethyl-2,3-bis(oleoyloxy)propan-1-aminium methylsulfate (DOTAP) and 1,1'-dioctadecyl-3, 3, 3', 3'-tetramethylindotricarbocyanineiodide (DiR') were prepared in chloroform with a ratio of 1:1:0.1 (w/w/w). Chloroform was removed under vacuum. 60 µg dried lipids were resuspended in PBS (0.15 mL), pH 7.4, containing 12 µg FABP5 construct. The suspension was mixed thoroughly and sonicated for 5 min on ice. The suspension was passed through the Whatman Nuclepore Track-Etch membrane with 0.1 µm pore size using an AVANTI Polar Lipids extruder. Liposomes with encapsulated proteins were purified via gel filtration with NAP5 columns (Cytiva).

Protein delivery. Cells in a 10 cm dish were washed with 1xPBS. EMEM medium was added and incubated at 37 °C for 30 mins. 0.15 mL of PBS solutions containing fusogenic liposomes without or with FABP5 construct were diluted with 0.15 mL EMEM. 0.15 mL of the diluted solutions were added to cells. Cells were incubated at room temperature or

37 °C for 1 h. Cells were washed with 1xPBS (1 mL x 4). Cells were lysed for western blot to confirm delivery. For migration assay, EMEM medium (without FBS and Pen-Strep) was added, followed by 50 μM linoleic acid. Cells were incubated at 37 °C for 24 h.

Western blot. Cells were lysed in ice-cold RIPA buffer (300 μL per 10 cm dish). After incubation at 4 °C for 30 min and centrifugation at 16,000 x g for 10 min at 4 °C, the supernatant was collected. The protein concentration was determined by Bradford assay. Proteins or lysates were separated by SDS-PAGE (12%) and transferred to the PVDF membrane. The membrane was blocked with 5 % BSA in Tris-buffered saline with 0.1% tween (TBST) and incubated with the following primary antibodies: FLAG (Sigma-Aldrich, F1804, 1:1000), glutathione (Virogen, 101-A-250, 1:1000), β-actin (Santa Cruz Biotechnology, sc-8432, 1:1000), GAPDH (Cell signaling, D4C6R, 1: 1000), and Lamin B1 (Cell signaling, D4Q4Z, 1: 1000). The membrane was then incubated with horseradish peroxidase (HRP)-conjugated anti-mouse IgG (NA931V, Sigma, 1:1000) and anti-Rabbit IgG, (NA934V, Sigma, 1:2000) to visualize the proteins by chemiluminescence (SuperSignal West Pico). Blots were imaged using the iBright imaging system (Thermo Scientific).

Cytoplasmic and nuclear extraction. Cytoplasmic and nuclear proteins were extracted using NE-PER™ Nuclear and Cytoplasmic Extraction Reagents (Thermo Scientific, 78833). Cells were harvested with trypsin-EDTA and centrifuged at 500 × g for 5 min. Cells were washed with 1xPBS and pelleted by centrifugation at 500 × g for 3 min. The cell pellet was dried and mixed with 500 μL of ice-cold cytoplasmic extraction reagent I

(CER I), followed by 27.5 µL of ice-cold cytoplasmic extraction reagent II (CER II). After incubating for 1 min, the sample was centrifuged for 5 min at 16,000 × g. The supernatant was collected as cytoplasmic extracts. The insoluble (pellet) fraction was suspended and lysed in 250 µL ice-cold nuclear extraction reagent (NER). After centrifugation at 16,000 × g for 10 minutes, the supernatant was collected as nuclear extracts.

PPARβ/δ activation. The method was adapted from prior work.[48] PPARβ/δ transcriptional activation was performed using the transcriptional factor assay kit (Abcam, ab133106). After protein delivery, the MCF7 nuclear extracts were prepared and mixed with the complete transcription factor binding assay buffer (CTFB), which was added to a 96-well plate immobilized with peroxisome proliferator response element (PPRE) and incubated at 4 °C. After washing with wash buffer (x5), each well in the plate was incubated with PPARβ/δ antibody (Abcam, AB133106, 1:1000) in binding buffer for 1 h at room temperature. After washing with wash buffer (x5), anti-rabbit HRP conjugate (Abcam, AB133106) was incubated for 1 h at room temperature. After incubating developing and stop solutions (colorimetric measurement), the bound PPARβ/δ was quantified by reading absorbance at 450 nm using a microplate reader (BioTek plate reader).

Migration assay. MCF-7 cells were seeded into 12 well plates coated with fibronectin/gelatin to produce a fully confluent monolayer (1.4 x 10^5 cells). After overnight, the monolayer cells were scratched using a 10 µL pipet tip to create an even wound. Cells were washed with warm PBS (1 mL x 4) to remove non-adherent cells and incubated in

EMEM for 30 min. 50 µL of fusogenic liposome diluted with 50 µL EMEM medium was added to cells, followed by incubating at 37 °C for 1 h. After washing with PBS (1 mL x 4), 50 µM linoleic acid was added to cells in EMEM, and cells were incubated at 37 °C. The wound area was imaged at 0 and 24 h using a light microscope connected to a camera. Images were analyzed using an MRI wound healing tool in ImageJ software.

NUT gel electrophoresis. Neutral pH urea Triton-polyacrylamide gel electrophoresis (NUT gel) was prepared according to the prior work.[35] NUT gel (15% resolving) was prepared and run with NUT-PAGE running buffer (22 mM MOPS pH 7.0, 100 mM imidazole). The samples were run at 125 V for 20 min, then at 100 V for 12 h at room temperature. The dhG-modified and non-modified peptides were visualized by fluorescence using the iBright imager (Thermo Scientific) and quantified using ImageJ software.

Kinetic analysis of dhG modification. Time-dependent samples at three different concentrations of dhG (100, 200, and 400 µM) were resolved on NUT-gels. The amounts of the peptide (starting peptide) remaining at different time points were quantified using ImageJ software. The logarithm values of the starting peptide at different times were plotted for reaction rates. Reactions were assumed to follow a pseudo-first-order kinetic mechanism. Reaction rates were plotted as a function of dhG concentrations. The second-order rate constant of dhG was obtained from the linear curve.

Statistical analysis. All data are shown with the means ± SD and analyzed by one-way or two-way ANOVA followed by Tukey's *post-hoc* test. The value $p < 0.03$ is statistically significant.

Data availability. All data supporting the findings of this study are available from the corresponding author upon request.

Supplementary information. This article contains supporting information, including the dhG synthesis scheme, peptide reaction with dhG, purification of FABP5 constructs, in vitro dhG modification of FABP5, ITC of FABP5 upon GSSG modification, FABP5 localization by fusogenic liposome, and additional experimental methods.

Acknowledgements

This work was supported by the National Institutes of Health (NIH) grant, R01 GM143214 (Y.-H.A.), and Drexel University. We would like to thank all the Ahn group members for assisting in the experiments. We thank Dr. Martin Kaczocha (Stony Brook University) for sharing FABP5 plasmids.

Author Contributions

Daniel Oppong: Formal Analysis, Investigation, Visualization, Writing – original draft, Writing – review & editing. **Rayavarapu Padmavathi**: Formal Analysis, Investigation, Visualization, Writing – original draft, Writing – review & editing. **Dhanushika Kukulage**: Conceptualization, Formal Analysis, Investigation, Writing – review & editing. **Madhu**

Shivamadhu: Investigation, Visualization, Writing – review & editing. **Elizabeth Newberry**: Formal Analysis. Writing – review & editing. **Anneliese Faustino**: Formal Analysis, Investigation, Visualization, Writing – review & editing. **Hsin-Yao Tang**: Supervision, Writing – review & editing. **Young-Hoon Ahn**: Conceptualization, Formal Analysis, Supervision, Visualization, Writing – original draft, Writing – review & editing, Funding Acquisition.

Competing Interests

The authors declare that they have no conflicts of interest with the contents of this article.

References

1. Pace, N. J.; Weerapana, E. Diverse functional roles of reactive cysteines. *ACS Chem Biol* **2013**, *8* (2), 283-296. DOI: 10.1021/cb3005269.
2. Fomenko, D. E.; Marino, S. M.; Gladyshev, V. N. Functional diversity of cysteine residues in proteins and unique features of catalytic redox-active cysteines in thiol oxidoreductases. *Mol Cells* **2008**, *26* (3), 228-235.
3. Paulsen, C. E.; Carroll, K. S. Cysteine-Mediated Redox Signaling: Chemistry, Biology, and Tools for Discovery. *Chem Rev* **2013**, *113* (7), 4633-4679.
4. Kukulage, D. S. K.; Samarasinghe, K. T. G.; Matarage Don, N. N. J.; Shivamadhu, M. C.; Shishikura, K.; Schiff, W.; Mashhadi Ramezani, F.; Padmavathi, R.; Matthews, M. L.; Ahn, Y. H. Protein phosphatase PP2Calpha S-glutathionylation regulates cell migration. *J Biol Chem* **2024**, 107784. DOI: 10.1016/j.jbc.2024.107784.
5. Truong, T. H.; Carroll, K. S. Redox regulation of epidermal growth factor receptor signaling through cysteine oxidation. *Biochemistry* **2012**, *51* (50), 9954-9965. DOI: 10.1021/bi301441e.
6. Behring, J. B.; van der Post, S.; Mooradian, A. D.; Egan, M. J.; Zimmerman, M. I.; Clements, J. L.; Bowman, G. R.; Held, J. M. Spatial and temporal alterations in protein structure by EGF regulate cryptic cysteine oxidation. *Sci Signal* **2020**, *13* (615). DOI: 10.1126/scisignal.aay7315.
7. Miki, H.; Funato, Y. Regulation of intracellular signalling through cysteine oxidation by reactive oxygen species. *J Biochem* **2012**, *151* (3), 255-261. DOI: 10.1093/jb/mvs006.
8. Yapa Abeywardana, M.; Samarasinghe, K. T. G.; Munkanatta Godage, D.; Ahn, Y. H. Identification and Quantification of Glutathionylated Cysteines under Ischemic

Stress. *J Proteome Res* **2021**, *20* (9), 4529-4542. DOI: 10.1021/acs.jproteome.1c00473.
9. Samarasinghe, K. T. G.; Godage, D. N. P. M.; Zhou, Y. N.; Ndombera, F. T.; Weerapana, E.; Ahn, Y. H. A clickable glutathione approach for identification of protein glutathionylation in response to glucose metabolism. *Mol Biosyst* **2016**, *12* (8), 2471-2480.
10. Ullevig, S.; Zhao, Q. W.; Lee, C. F.; Kim, H. S.; Zamora, D.; Asmis, R. NADPH Oxidase 4 Mediates Monocyte Priming and Accelerated Chemotaxis Induced by Metabolic Stress. *Arterioscl Throm Vas* **2012**, *32* (2), 415-426.
11. Tew, K. D.; Townsend, D. M. Redox platforms in cancer drug discovery and development. *Curr Opin Chem Biol* **2011**, *15* (1), 156-161.
12. Uys, J. D.; Manevich, Y.; DeVane, L. C.; He, L.; Garret, T. E.; Pazoles, C. J.; Tew, K. D.; Townsend, D. M. Preclinical pharmacokinetic analysis of NOV-002, a glutathione disulfide mimetic. *Biomed Pharmacother* **2010**, *64* (7), 493-498.
13. Dewey, D. L.; Beecher, J. Interconversion of cystine and cysteine induced by x-rays. *Nature* **1965**, *206* (991), 1369-1370. DOI: 10.1038/2061369a0.
14. Taylor, J. E.; Yan, J. F.; Wang, J. L. The iron(3)-catalyzed oxidation of cysteine by molecular oxygen in the aqueous phase. An example of a two-thirds-order reaction. *J Am Chem Soc* **1966**, *88* (8), 1663-1667. DOI: 10.1021/ja00960a016.
15. Ortiz de Orue Lucana, D.; Roscher, M.; Honigmann, A.; Schwarz, J. Iron-mediated oxidation induces conformational changes within the redox-sensing protein HbpS. *J Biol Chem* **2010**, *285* (36), 28086-28096. DOI: 10.1074/jbc.M110.127506.
16. Gould, N. S.; Evans, P.; Martinez-Acedo, P.; Marino, S. M.; Gladyshev, V. N.; Carroll, K. S.; Ischiropoulos, H. Site-Specific Proteomic Mapping Identifies Selectively Modified Regulatory Cysteine Residues in Functionally Distinct Protein Networks. *Chem Biol* **2015**, *22* (7), 965-975. DOI: 10.1016/j.chembiol.2015.06.010.
17. Kukulage, D. S. K.; Matarage Don, N. N. J.; Ahn, Y. H. Emerging chemistry and biology in protein glutathionylation. *Curr Opin Chem Biol* **2022**, *71*, 102221. DOI: 10.1016/j.cbpa.2022.102221.
18. Oppong, D.; Schiff, W.; Shivamadhu, M. C.; Ahn, Y. H. Chemistry and biology of enzymes in protein glutathionylation. *Curr Opin Chem Biol* **2023**, *75*, 102326. DOI: 10.1016/j.cbpa.2023.102326.
19. Lee, C. F.; Ullevig, S.; Kim, H. S.; Asmis, R. Regulation of Monocyte Adhesion and Migration by Nox4. *Plos One* **2013**, *8* (6), e66964.
20. Mullen, L.; Mengozzi, M.; Hanchmann, E. M.; Alberts, B.; Gjezzo, P. How the redox state regulates immunity. *Free Radic Biol Med* **2020**, *157*, 3-14. DOI: 10.1016/j.freeradbiomed.2019.12.022.
21. Chia, S. B.; Nolin, J. D.; Aboushousha, R.; Erikson, C.; Irvin, C. G.; Poynter, M. E.; van der Velden, J.; Taatjes, D. J.; van der Vliet, A.; Anathy, V.; Janssen-Heininger, Y. M. W. Glutaredoxin deficiency promotes activation of the transforming growth factor beta pathway in airway epithelial cells, in association with fibrotic airway remodeling. *Redox Biol* **2020**, *37*, 101720. DOI: 10.1016/j.redox.2020.101720.
22. Alegre-Cebollada, J.; Kosuri, P.; Giganti, D.; Eckels, E.; Rivas-Pardo, J. A.; Hamdani, N.; Warren, C. M.; Solaro, R. J.; Linke, W. A.; Fernandez, J. M. S-

Glutathionylation of Cryptic Cysteines Enhances Titin Elasticity by Blocking Protein Folding. *Cell* **2014**, *156* (6), 1235-1246.
23. Adachi, T.; Weisbrod, R. M.; Pimentel, D. R.; Ying, J.; Sharov, V. S.; Schoneich, C.; Cohen, R. A. S-Glutathiolation by peroxynitrite activates SERCA during arterial relaxation by nitric oxide. *Nat Med* **2004**, *10* (11), 1200-1207. DOI: 10.1038/nm1119.
24. Cha, S. J.; Kim, H.; Choi, H. J.; Lee, S.; Kim, K. Protein Glutathionylation in the Pathogenesis of Neurodegenerative Diseases. *Oxid Med Cell Longev* **2017**, *2017*, 2818565. DOI: 10.1155/2017/2818565.
25. Hayes, J. D.; Dinkova-Kostova, A. T.; Tew, K. D. Oxidative Stress in Cancer. *Cancer Cell* **2020**, *38* (2), 167-197. DOI: 10.1016/j.ccell.2020.06.001.
26. Kukulage, D. S. K.; Yapa Abeywardana, M.; Matarage Don, N. N. J.; Hu, R. M.; Shishikura, K.; Matthews, M. L.; Ahn, Y. H. Chemoproteomic strategy identified p120-catenin glutathionylation regulates E-cadherin degradation and cell migration. *Cell Chem Biol* **2023**, *30* (12), 1542-1556 e1549. DOI: 10.1016/j.chembiol.2023.08.004.
27. Munkanatta Godage, D. N. P.; VanHecke, G. C.; Samarasinghe, K. T. G.; Feng, H. Z.; Hiske, M.; Holcomb, J.; Yang, Z.; Jin, J. P.; Chung, C. S.; Ahn, Y. H. SMYD2 glutathionylation contributes to degradation of sarcomeric proteins. *Nat Commun* **2018**, *9* (1), 4341. DOI: 10.1038/s41467-018-06786-x.
28. Xu, B.; Chen, L.; Zhan, Y.; Marquez, K. N. S.; Zhuo, L.; Qi, S.; Zhu, J.; He, Y.; Chen, X.; Zhang, H.; Shen, Y.; Chen, G.; Gu, J.; Guo, Y.; Liu, S.; Xie, T. The Biological Functions and Regulatory Mechanisms of Fatty Acid Binding Protein 5 in Various Diseases. *Front Cell Dev Biol* **2022**, *10*, 857919. DOI: 10.3389/fcell.2022.857919.
29. George Warren, W.; Osborn, M.; Yates, A.; Wright, K.; O'Sullivan, S. E. The emerging role of fatty acid binding protein 5 (FABP5) in cancers. *Drug Discov Today* **2023**, *28* (7), 103628. DOI: 10.1016/j.drudis.2023.103628.
30. Odani, S.; Namba, Y.; Ishii, A.; Ono, T.; Fujii, H. Disulfide bonds in rat cutaneous fatty acid-binding protein. *J Biochem* **2000**, *128* (3), 355-361. DOI: 10.1093/oxfordjournals.jbchem.a022761.
31. Guo, Y.; Liu, Y.; Zhao, S.; Xu, W.; Li, Y.; Zhao, P.; Wang, D.; Cheng, H.; Ke, Y.; Zhang, X. Oxidative stress-induced FABP5 S-glutathionylation protects against acute lung injury by suppressing inflammation in macrophages. *Nat Commun* **2021**, *12* (1), 7094. DOI: 10.1038/s41467-021-27428-9.
32. Hohoff, C.; Borchers, T.; Rustow, B.; Spener, F.; van Tilbeurgh, H. Expression, purification, and crystal structure determination of recombinant human epidermal-type fatty acid binding protein. *Biochemistry* **1999**, *38* (38), 12229-12239. DOI: 10.1021/bi990305u.
33. Asquith, R. S.; Carthew, P. The preparation and subsequent identification of a dehydroalanyl peptide from alkali-treated oxidised glutathione. *Biochim Biophys Acta* **1972**, *285* (2), 346-351. DOI: 10.1016/0005-2795(72)90319-4.
34. Sauerland, M.; Mertes, R.; Morozzi, C.; Eggler, A. L.; Gamon, L. F.; Davies, M. J. Kinetic assessment of Michael addition reactions of alpha, beta-unsaturated carbonyl compounds to amino acid and protein thiols. *Free Radic Biol Med* **2021**, *169*, 1-11. DOI: 10.1016/j.freeradbiomed.2021.03.040.

35. Buehl, C. J.; Deng, X.; Liu, M.; McAndrew, M. J.; Hovde, S.; Xu, X.; Kuo, M. H. Resolving acetylated and phosphorylated proteins by neutral urea Triton-polyacrylamide gel electrophoresis: NUT-PAGE. *Biotechniques* **2014**, *57* (2), 72-80. DOI: 10.2144/000114197.
36. Yang, J.; Gupta, V.; Carroll, K. S.; Liebler, D. C. Site-specific mapping and quantification of protein S-sulphenylation in cells. *Nat Commun* **2014**, *5*, 4776. DOI: 10.1038/ncomms5776.
37. Armstrong, E. H.; Goswami, D.; Griffin, P. R.; Noy, N.; Ortlund, E. A. Structural basis for ligand regulation of the fatty acid-binding protein 5, peroxisome proliferator-activated receptor beta/delta (FABP5-PPARbeta/delta) signaling pathway. *J Biol Chem* **2014**, *289* (21), 14941-14954. DOI: 10.1074/jbc.M113.514646.
38. Kube, S.; Hersch, N.; Naumovska, E.; Gensch, T.; Hendriks, J.; Franzen, A.; Landvogt, L.; Siebrasse, J. P.; Kubitscheck, U.; Hoffmann, B.; Merkel, R.; Csiszar, A. Fusogenic Liposomes as Nanocarriers for the Delivery of Intracellular Proteins. *Langmuir* **2017**, *33* (4), 1051-1059. DOI: 10.1021/acs.langmuir.6b04304.
39. Levi, L.; Wang, Z.; Doud, M. K.; Hazen, S. L.; Noy, N. Saturated fatty acids regulate retinoic acid signalling and suppress tumorigenesis by targeting fatty acid-binding protein 5. *Nat Commun* **2015**, *6*, 8794. DOI: 10.1038/ncomms9794.
40. Ganley, I. G.; Carroll, K.; Bittova, L.; Pfeffer, S. Rab9 GTPase regulates late endosome size and requires effector interaction for its stability. *Mol Biol Cell* **2004**, *15* (12), 5420-5430. DOI: 10.1091/mbc.e04-08-0747.
41. Tan, N. S.; Shaw, N. S.; Vinckenbosch, N.; Liu, P.; Yasmin, R.; Desvergne, B.; Wahli, W.; Noy, N. Selective cooperation between fatty acid binding proteins and peroxisome proliferator-activated receptors in regulating transcription. *Mol Cell Biol* **2002**, *22* (14), 5114-5127. DOI: 10.1128/MCB.22.14.5114-5127.2002.
42. Stephen, R. L.; Gustafsson, M. C.; Jarvis, M.; Tatoud, R.; Marshall, B. R.; Knight, D.; Ehrenborg, E.; Harris, A. L.; Wolf, C. R.; Palmer, C. N. Activation of peroxisome proliferator-activated receptor delta stimulates the proliferation of human breast and prostate cancer cell lines. *Cancer Res* **2004**, *64* (9), 3162-3170. DOI: 10.1158/0008-5472.can-03-2760.
43. Morgan, E.; Kannan-Thulasiraman, P.; Noy, N. Involvement of Fatty Acid Binding Protein 5 and PPARbeta/delta in Prostate Cancer Cell Growth. *PPAR Res* **2010**, *2010*. DOI: 10.1155/2010/234629.
44. Chalker, J. M.; Bernardes, G. J.; Davis, B. G. A "tag-and-modify" approach to site-selective protein modification. *Acc Chem Res* **2011**, *44* (9), 730-741. DOI: 10.1021/ar200056q.
45. Bernardes, G. J.; Chalker, J. M.; Errey, J. C.; Davis, B. G. Facile conversion of cysteine and alkyl cysteines to dehydroalanine on protein surfaces: versatile and switchable access to functionalized proteins. *J Am Chem Soc* **2008**, *130* (15), 5052-5053. DOI: 10.1021/ja800800p.
46. Yang, J.; Gupta, V.; Carroll, K. S.; Liebler, D. C. Site-specific mapping and quantification of protein S-sulphenylation in cells. *Nat Commun* **2014**, *5,* 4776.
47. Wang, Q.; Rizk, S.; Bernard, C.; Lai, M. P.; Kam, D.; Storch, J.; Stark, R. E. Protocols and pitfalls in obtaining fatty acid-binding proteins for biophysical studies

of ligand-protein and protein-protein interactions. *Biochem Biophys Rep* **2017**, *10*, 318-324. DOI: 10.1016/j.bbrep.2017.05.001.
48. Mori, C.; Lee, J. Y.; Tokumoto, M.; Satoh, M. Cadmium Toxicity Is Regulated by Peroxisome Proliferator-Activated Receptor delta in Human Proximal Tubular Cells. *Int J Mol Sci* **2022**, *23* (15). DOI: 10.3390/ijms23158652.

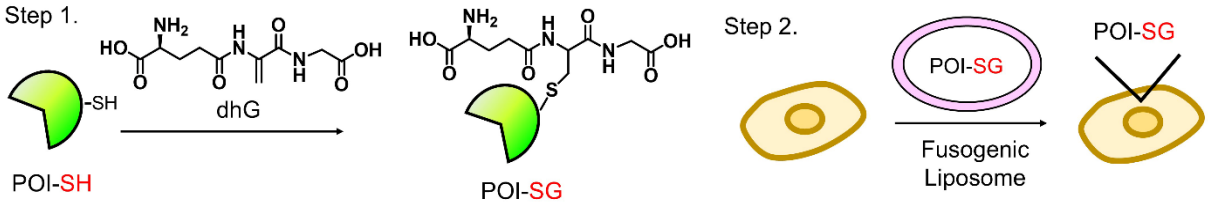

Figure 1. G-PROV approach for functional study of glutathionylated proteins in cells. The protein of interest (POI) is subjected to a reaction with dehydroglutathione (dhG) in vitro, which induces a non-reducible mimic of glutathionylation (step 1). The dhG-mediated glutathione-modified POI is delivered to the cytoplasm of cells via fusogenic liposome for functional phenotype analysis.

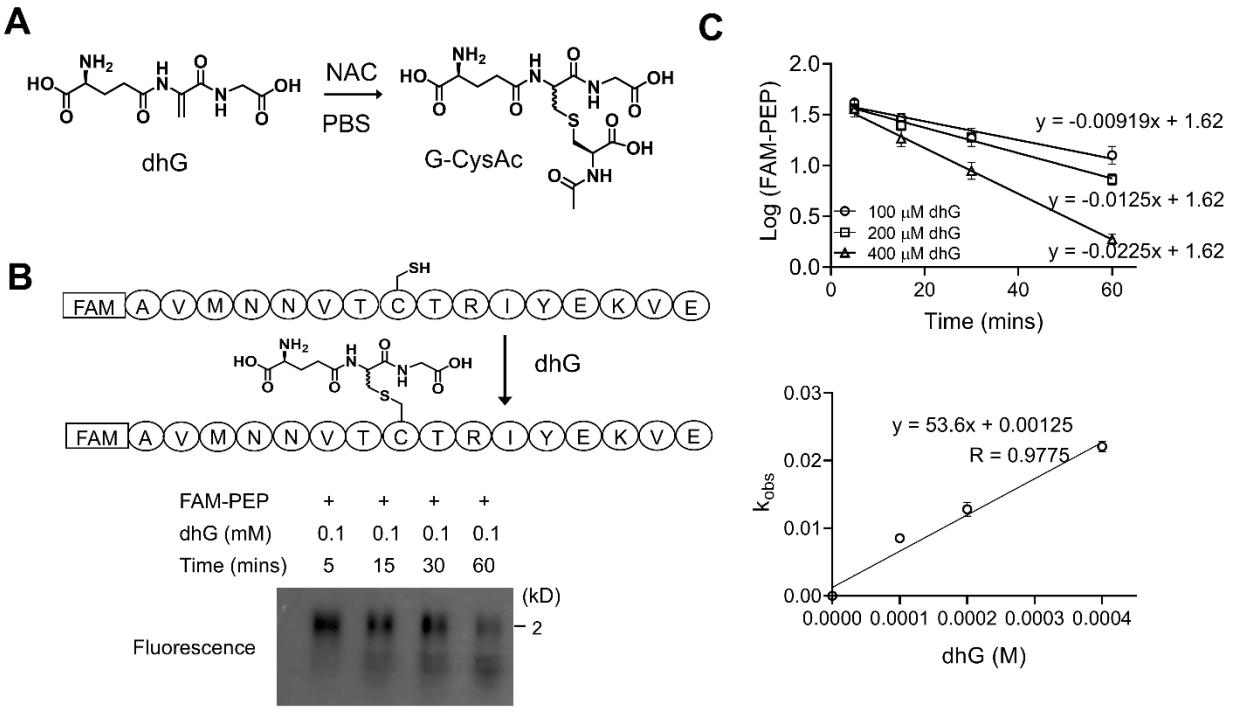

Figure 2. dhG reaction with Cys results in a thioether linkage of glutathione modification. (A) dhG reaction with Cys, resulting in the Michael reaction adduct. (B) The reaction of fluorescein-conjugated Cys-containing peptide (FAM-PEP) with dhG in urea-gel electrophoresis (n=3). FAM-PEP and its conjugation product were monitored by fluorescence. (C) dhG reaction kinetics with FAM-PEP. The intensities of FAM-PEP bands at different times were plotted for the rate (top). Reactions were assumed to follow pseudo-first-order kinetics. Reaction rates were plotted as a function of dhG concentrations (bottom) to determine the second-order rate constant (n=3). Data show the mean ± SD or representative of replicate experiments.

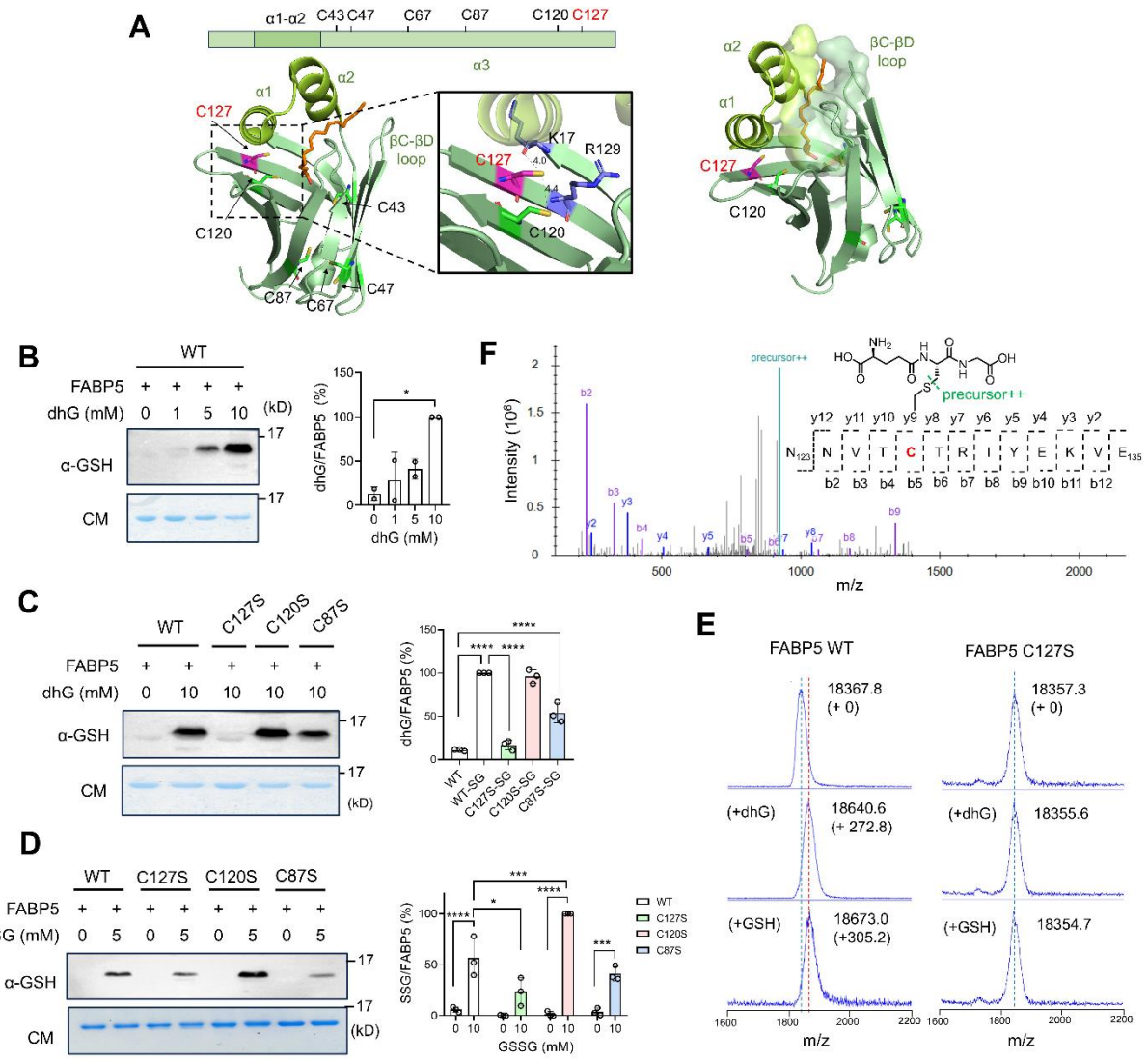

Figure 3. dhG induces glutathione modification on C127 of FABP5. (A) FABP5 structure (PDB: 4LKT) with positions of 6 cysteine residues. FABP5 has a twisted β-barrel structure with two helices (α1 and α2) acting as a lid (left). An enlarged structure around C127 with residues in proximity (middle). The size and depth of the lipid-binding pocket in FABP5 (right). Linoleic acid is shown in a stick model (orange). (B) dhG-modification on FABP5 WT. Increasing amounts of dhG were incubated with purified FABP5 in PBS, which was analyzed by Coomassie stain (CM) and glutathione antibody (α-GSH) (n=2). (C) dhG-modification on FABP5 WT and cysteine mutants (n=3). (D) GSSG-mediated S-

glutathionylation of FABP5 WT and cysteine mutants. Purified FABP5 constructs were incubated with GSSG for 1 h (n=3). (E) MALDI-TOF analysis of FABP5 WT or C127S incubated with dhG or GSSG. FABP5 constructs were incubated for dhG (10 mM) or GSSG (5 mM) for 1 h (n=3). (F) MS2 spectrum of a dhG-modified peptide in FABP5. FABP5 modified by dhG was digested by CNBr and analyzed by LC-MS/MS, finding a peptide modified by dhG at C127. Data show the mean ± SD or representative of replicate experiments. The statistical difference was analyzed by one-way (B-C) or two-way (D) ANOVA with Tukey's post-hoc test, where *$p < 0.03$, **$p < 0.002$, ***$p < 0.0002$, ****$p < 0.0001$.

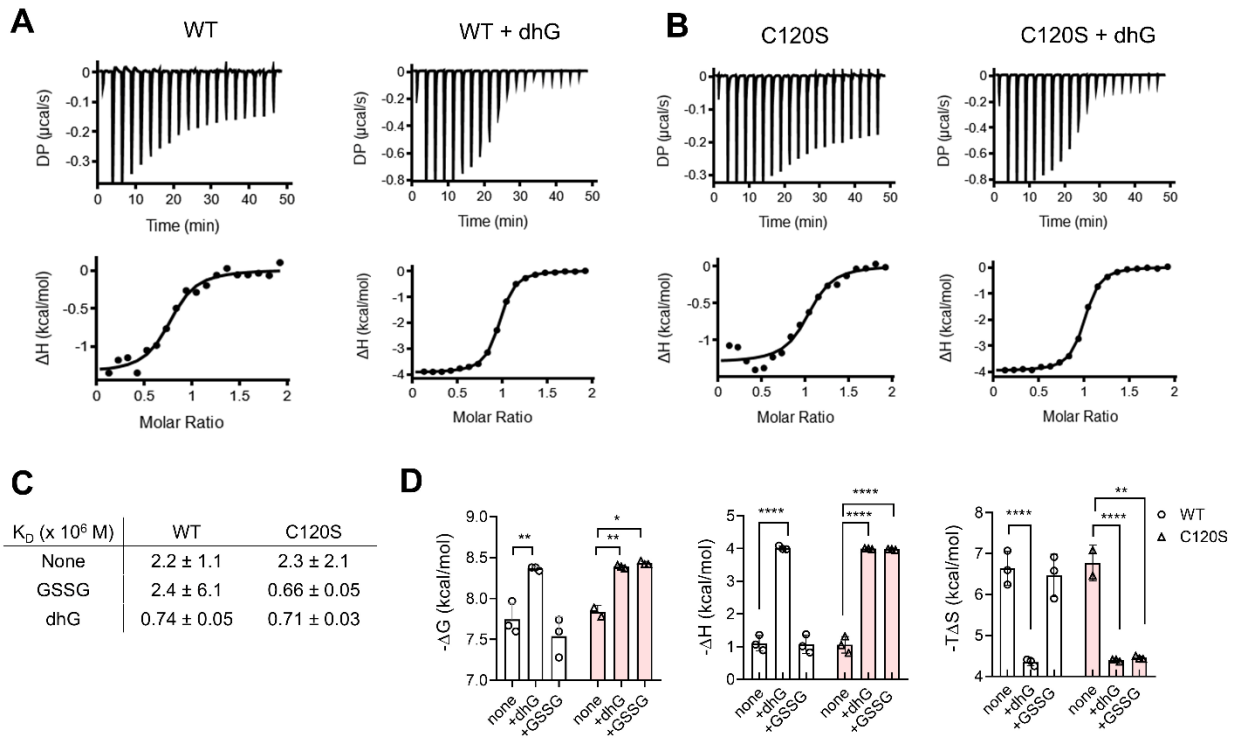

K_D (x 10^6 M)	WT	C120S
None	2.2 ± 1.1	2.3 ± 2.1
GSSG	2.4 ± 6.1	0.66 ± 0.05
dhG	0.74 ± 0.05	0.71 ± 0.03

Figure 4. dhG-modification of FABP5 increases the binding affinity to linoleic acid. (A-B) The isothermal titration calorimetry (ITC) to measure FABP5 binding affinity with linoleic acid (LA) upon dhG modification. FABP5 WT (A) and C120S (B) without or with incubation of dhG (10 mM) were purified before the measurement by ITC (n=3). The differential power (DP) was measured while LA (1 mM) was added to FABP5 (0.1 mM) in Tris-HCl, pH 7.4, over time. (C) The summary of the binding affinity between LA and FABP5 constructs without or with modification by dhG or GSSG. (D) The thermodynamic parameters of FABP5 binding interactions to LA. Data show the mean ± SD or representative of 2-3 independent experiments. The statistical difference was analyzed by two-way ANOVA with Tukey's post-hoc test, where *p < 0.03, **p < 0.002, ***p < 0.0002, ****p < 0.0001.

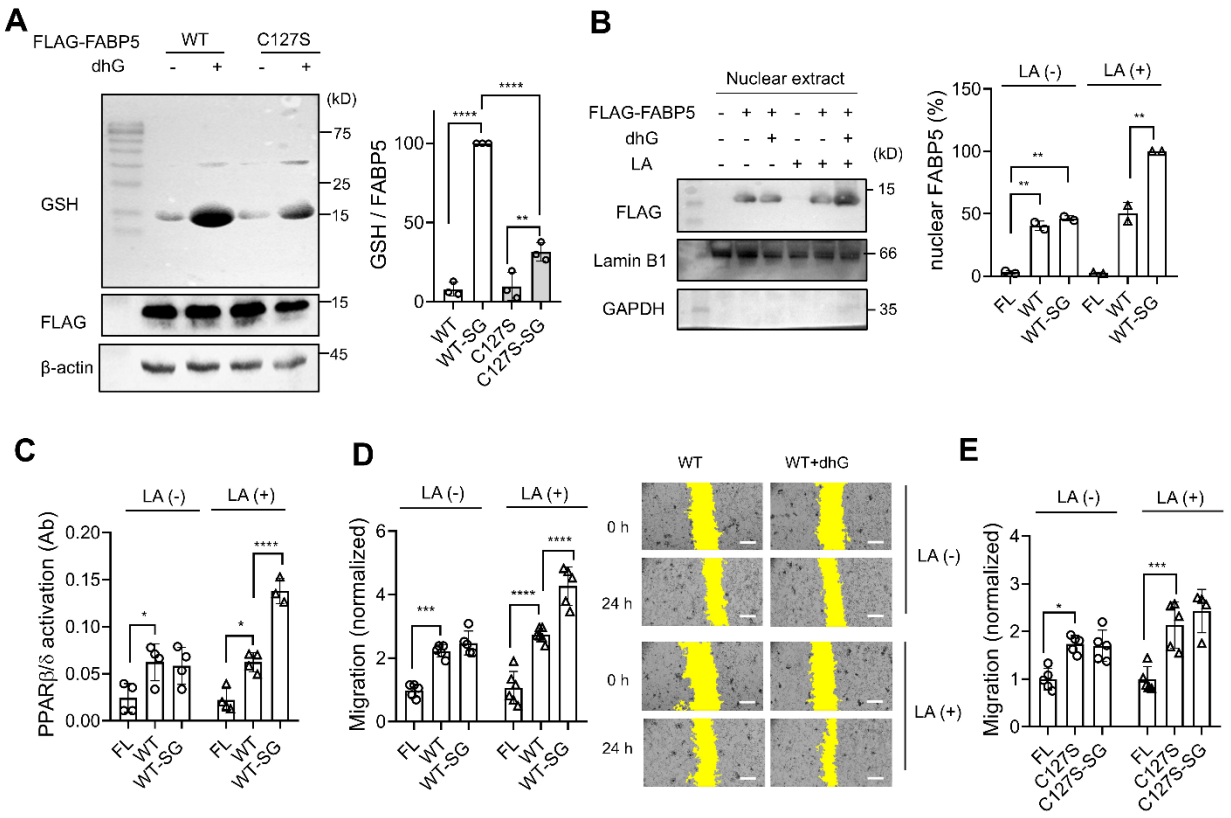

Figure 5. FABP5 glutathione modification increases its nuclear translocation, PPARβ/δ activation, and MCF7 cell migration in response to linoleic acid. Fusogenic liposomes alone (FL) or containing FABP5 WT or C127S without or with dhG modification were incubated in MCF7 cells for 1 h. (A) Analysis of FABP5 in MCF7 cells after incubating fusogenic liposome. Lysates were analyzed by western blots (n=3). (B) FABP5 nuclear level upon adding LA. MCF7 cells were treated with none or LA for 12 h. MCF7 cells were lysed, and nuclear extracts were analyzed by western blots (n=2). (C) PPARβ/δ activation upon adding LA. After incubating LA for 12 h, the nuclear extracts were collected, and the levels of PPARβ/δ bound to the peroxisome proliferator response element (PPRE) were measured by absorbance (n=4). (D-E) The in-vitro scratch migration assays of MCF7 cells upon incubating LA for 24 h. After incubating fusogenic liposomes containing FABP5 WT (D) or C127S (E), MCF7 cells were incubated without

or with LA. The images were taken at 0 and 24 h (n=5). Yellow colors indicate the area without cells. A scale bar = 0.5 mm. Data show the mean ± SD or representative of replicate experiments. The statistical difference was analyzed by one-way (A-B) or two-way (C-E) ANOVA and Tukey's post-hoc test, where *$p < 0.03$, **$p < 0.002$, ***$p < 0.0002$, ****$p < 0.0001$.